Magnetospheric Radio Sounding on the IMAGE Mission

Robert F. Benson et al.

Abstract

Radio sounding can be used to obtain accurate remote, as well as *in situ*, electron number density (N_e) measurements in magnetized space plasmas. It is based on the reflection of radio waves at the location where the refractive index goes to zero. The N_e structure of the terrestrial ionosphere has been routinely investigated by both ground-based and satellite-borne sounders. The terrestrial magnetosphere, on the other hand, has never been subject to routine radio-sounding investigations.

Recently, NASA selected Imager for Magnetopause-to-Aurora Global Exploration (IMAGE) as the first Medium-class-Explorer (MIDEX) mission. IMAGE is scheduled to be launched on January 1, 2000 and has the scientific objective of understanding the global dynamics of the terrestrial magnetosphere and its response to changing solar-wind conditions. The IMAGE payload includes a radio plasma imager (RPI) in addition to far ultraviolet (FUV), extreme ultraviolet (EUV) and neutral atom (NAI) imagers. The RPI will consist of a swept-frequency digital radio sounder covering the frequency range from 3 kHz to 3 MHz. It will be designed similar to modern state-of-the-art ground-based digital ionospheric sounders. It will employ on-board digital signal-processing techniques and will be capable of measuring echo amplitude, phase, time delay, Doppler spectrum, polarization and direction-of-arrival as a function of sounding frequency. Most RPI soundings will be taken near apogee at a geocentric distance of 8 R_E between 45 and 90° north geographic latitude. In this region, the spacecraft will be immersed in the N_e cavity extending from the plasmapause to the magnetopause. The RPI will often be able to

Drs. R. F. Benson, J. L. Green and S. F. Fung are with the NASA Goddard Space Flight Center Greenbelt, Maryland 20771, U.S.A. Fax: (301) 286-1683

Drs. B. W. Reinisch, W. Calvert and D. M. Haines are with the Center for Atmospheric Research University of Massachusetts Lowell, Massachusetts 01854, U.S.A. Fax: (978) 459-7915

Drs. J.-L. Bougeret and R. Manning are with the Observatoire de Paris - Meudon F-92195 MEUDON Cedex, FRANCE Fax: 33-1-4507-2806

D. L. Carpenter is with the Electrical Engineering Dept. Stanford University Stanford, California 94305, U.S.A. Fax: (415)723-9251

Dr. D. L. Gallagher is with the NASA Marshall Space Flight Center Huntsville, Alabama 35812, U.S.A. Fax: (205) 544-5244

Dr. P. H. Reiff is with the Department of Space Physics and Astronomy Rice University Houston, Texas 77251-1892, U.S.A. Fax: (713) 285-5143

Dr. W. W. L. Taylor is with the Raytheon STX Corporation/ NASA Goddard Space Flight Center Greenbelt, Maryland 20771, U.S.A. Fax: (301)-286-1771

simultaneously determine the N_e profiles leading up to these two boundaries. In addition, it will be able to produce echo maps showing magnetospheric N_e structures. The combination of such information with the FUV, EUV and NAI images, will provide unprecedented global descriptions of magnetospheric dynamic plasma processes.

1. Introduction

The ionosphere and magnetosphere are the ionized (plasma) regions of the terrestrial atmosphere. Since the ionosphere is strongly influenced by the terrestrial magnetic field, it can be considered as part of the magnetosphere. Yet these two regions have often been investigated separately, the ionosphere mainly from the point-of-view of radiowave communication and the magnetosphere because of its interaction with the solar wind. These regions can be defined in a number of different ways, one being in terms of the motions of free electrons. The ionosphere is the region extending from about 60 to several thousand km where the motions of free electrons have a strong effect on medium-and high-frequency radiowave propagation. The magnetosphere is the region at higher altitudes (extending out to the boundary with the solar wind) where the terrestrial magnetic field dominates electron motions.

Both regions were experimentally confirmed using remote probing with radio waves prior to the advent of the space age in 1957. The ionospheric experiments were based on reflections of man-made radio waves [*Appleton and Barnett*, 1925; *Breit and Tuve*, 1926]. The magnetospheric experiments were based on the detection of naturally-produced (from lightning flashes) low-frequency waves (whistlers) that were guided from one hemisphere to the other along the direction of the Earth's magnetic field [*Storey*, 1953]. The lower portion of the ionosphere has since been routinely investigated from the ground using ionospheric radio sounders (ionosondes) based on the pulsed sounding technique of *Breit and Tuve* [1926]. The shielding effect of the ionosphere has prevented the conduct of similar routine ground-based sounding of the magnetosphere.

There have been compelling scientific and practical motivations for investigating the ionosphere and magnetosphere. The overall scientific objective has been to understand the underlying physics of these dynamic plasma regions of the terrestrial environment. An early practical motivation (long before the advent of communications satellites) was the optimization of long-distance radio communications. Another major one was to understand and possibly mitigate damaging effects due to magnetospheric substorms and magnetic storms which are characterized by enhanced currents in high and low-latitude plasma domains, respectively. These effects play havoc with communications systems, high-latitude power-line grids and pipelines, and the operations of man-made satellites and other high-technology systems. It has been argued that the original practical motivation for ionospheric research, i.e., long-distance radio communication, evaporated with the advent of communications satellites. This argument was not well accepted in areas (such as defense) where redundancy is of prime importance. Ironically, rather than eliminating the need for ionospheric research, advanced technology has emphasized its importance since the performance of state-of-the-art systems (e.g., the Global-Positioning-System satellites) are often limited by ionospheric dynamics. In the case of space-weather or solar-storm related effects, satellite operations are sometimes interrupted or even terminated. Such environmental effects may have contributed to the interruptions of television services dependent on the Canadian geostationary satellite Anik E-1 in January, 1994 and to the January, 1997 failure of the Telstar 401 satellite. From the scientific point-of-view, an improved understanding of the complex physics of the ionosphere and magnetosphere is not limited to the terrestrial system since an extrapolation of this knowledge will lead to a better understanding of the plasma environments of other planets.

2. Brief Review of Ionospheric Radio Sounding

The type of ionospheric radio sounding under discussion here is based on the reflection of short-duration radio pulses. This reflection occurs in a region where the transmitted radiowave frequency equals the local wave cutoff frequency for electron waves. The wave cutoff frequency depends on the propagation mode. To illustrate, consider a linearly-polarized wave transmit-

ted from the ground, and propagating with the wave vector **k** perpendicular to the direction of the terrestrial magnetic field **B**. In certain frequency ranges, it is broken into two modes in the presence of **B**. One of these has the wave electric field parallel to **B** and the wave propagates with linear polarization exactly the same as in the case of no background **B**. It is thus called the ordinary (O) mode. Since it can also exist outside of the plasma, it is also called a free-space mode. The other mode has the wave electric field perpendicular to **B** with a small component parallel to **k**. This elliptically-polarized wave is called the extraordinary wave which, in a plasma such as the ionosphere, has two branches. In ionospheric terminology they have been designated as the X mode (which, like the O mode, can exist in free-space) and the Z mode (which only exists within a plasma).

The O mode wave cutoff is equal to the ambient electron plasma frequency f_N (also commonly designated as f_p) which is related to the electron number density N_e and is given by

$$f_N \cong 9\,(N_e)^{1/2} \qquad (1)$$

when f_N is expressed in Hz and N_e in m^{-3} (or kHz and cm^{-3}, respectively). The X mode wave cutoff is designated as f_X, which is dependent on $|\mathbf{B}|$, and is related to f_N as follows:

$$f_X = (f_H/2)\,\{1 + (1+ 4\,f_N^2/f_H^2)^{1/2}\} \qquad (2)$$

where f_H is the electron gyrofrequency given by

$$f_H \cong 0.028\,|\mathbf{B}| \qquad (3)$$

when f_H is expressed in kHz and $|\mathbf{B}|$ in nT. The Z mode wave cutoff is designated as f_Z and is related to f_X by the following expression:

$$f_Z = (f_H/2)\,\{-1 + (1+ 4\,f_N^2/f_H^2)^{1/2}\} = f_X - f_H \qquad (4)$$

In the case of **k** parallel to **B**, there are two free-space modes which are circularly polarized, one with the wave electric field vector rotating in the right-hand sense (the R mode) and one rotating in the left-hand sense (the L mode). The wave cutoffs for the R and L modes are the same as for the X and Z modes given in (2) and (4), respectively.

In the more typical case of propagation oblique to **B**, there is a smooth transition between the free-space modes of parallel (R & L) and perpendicular (X & O) propagation. Thus the two free-space modes are often designated as the R-X and L-O modes (see, e.g., *Goertz and Strangeway* [1995]). In ionospheric terminology, these modes are often referred to as X and O even when the propagation direction is very nearly parallel to **B** (see, e.g., *Budden* [1985]).

Ionospheric sounding using ground-based ionosondes has been carried out for seven decades. A review of the evolution of the instrumentation over this period (which included the transformation from analog to digital instruments) is given in *Hunsucker* [1991]. Since this sounding is based on total reflection, only those signals reflected between the sounder and the location of the peak f_N can be returned during vertical-sounding experiments. This restriction limits the altitude range of vertical sounding. Thus ionospheric sounders have been classified as either ground-based or topside sounders. Ground-based sounders investigate the ionosphere up to the altitude of peak N_e (typically 300 km), whereas topside sounders investigate the region from the altitude of the spacecraft down to the altitude of the peak.

Topside ionospheric sounding has been performed by satellite-borne sounders for three and a half decades [*Jackson et al.*, 1980; *Jackson*, 1986]. The highly successful Alouette/ISIS program yielded more than 50 satellite-years of topside sounding operation and nearly 1,000 scientific publications based on analog sounders (recording echo amplitude and delay time as a function of frequency) designed by *Franklin and Maclean* [1969]. An effort is currently underway to convert selected Alouette/ISIS topside-sounder data from an analog to a digital format [*Benson*, 1996, see also http://nssdc.gsfc.nasa.gov/space/isis/isis-status.html]. Additional ionospheric topside sounders have been flown as described by *Pulinets* [1989]. Recently, a bistatic rocket experiment produced topside N_e profiles during active auroral conditions in addition to unique observations concerning wave propagation parallel to **B** and wave-particle interactions [*James*, 1996].

Figure 1 illustrates how the echoes received by ionospheric sounders are related to the vertical N_e distribution in an assumed horizontally-stratified

ionosphere. It is composed of four separate figures combined to illustrate how a complete ionospheric vertical N_e profile is produced from topside and ground-based ionosonde data. The data were simultaneously collected during a pass of the Alouette 1 satellite over Wallops Island, Virginia. The sounder data are presented in the form of echo time delay as a function of the sounder frequency. The time delay t is often expressed in terms of a virtual (or apparent) range given by ct/2, i.e., assuming that the propagation is at the free space speed of light c. The solid lines represent the O-mode traces as they appeared on the data records (called ionograms) from both the ground-based Wallops Island ionosonde and the Alouette 1 topside sounder (1,000 km altitude). One of the four figures used to make this composite consisted of the solid curves at the bottom which were obtained from the Wallops Island ionogram which displayed the virtual range (lower right axis) as a function of sounder frequency (bottom axis). These traces were produced by reflections from the ionospheric E and F regions. The second of the four figures used in the Figure 1 composite consisted of the solid curve starting at the top. It was obtained from the Alouette 1 ionogram which displayed the virtual range (top right axis) as a function of sounder frequency (bottom axis). The third and fourth figures used in this composite have been blended into one dashed line trace. It represents the vertical N_e distribution with true altitude (left scale) calculated from the ionosonde data. In order to aid in the comparison of the N_e profile with the ionogram traces, N_e has been converted to f_N (top scale) using (1). The portion of this profile below about 300 km altitude (with the E, F_1, and F_2 regions labeled) was derived from the Wallops Island ionosonde reflection labeled "Ground-Based Sounding Trace"; the portion above 300 km was derived from the Alouette 1 reflection

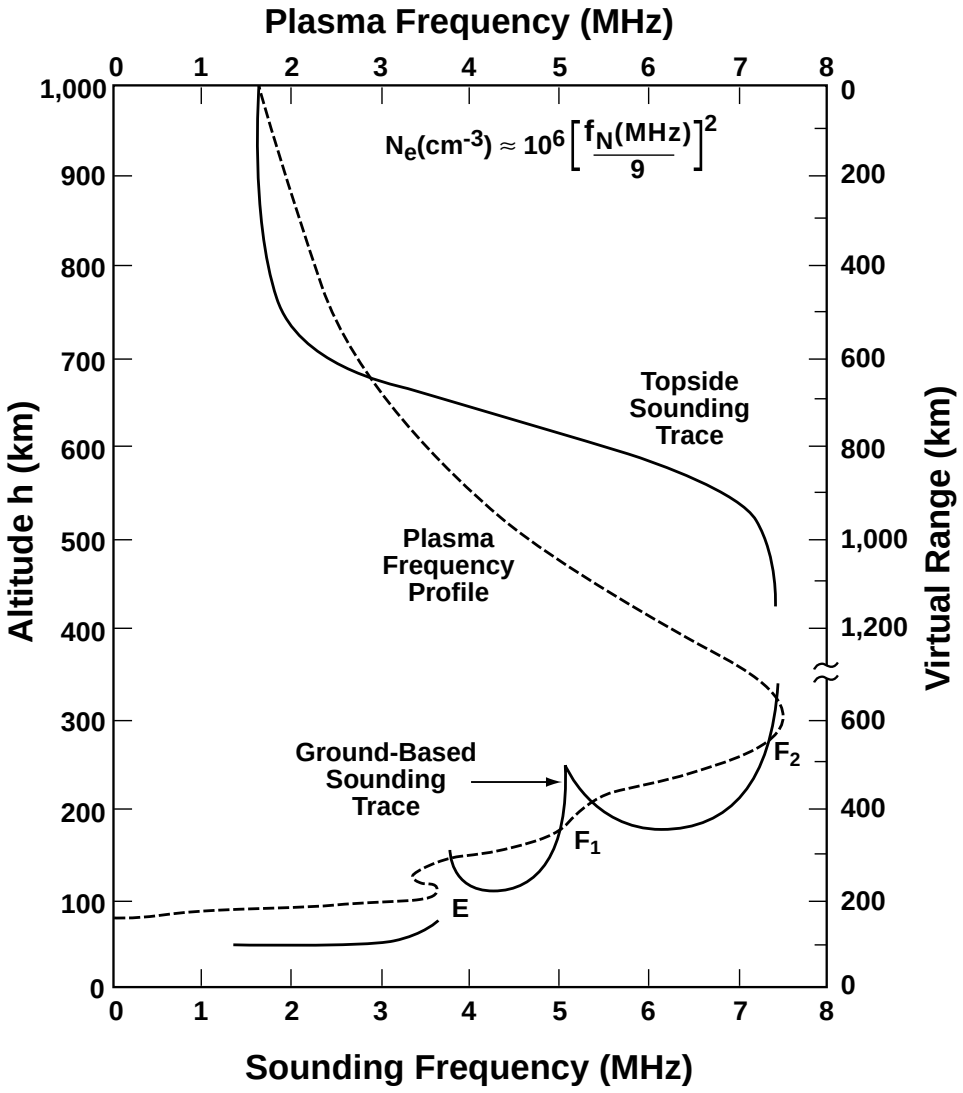

Figure 1. Vertical N_e profiles (dashed line) calculated from topside (Alouette 1) and ground-based (Wallops Island, Virginia) ionosonde O-mode traces (solid curves) presented in the form of virtual range (right scale). The vertical true height (left scale) N_e distribution is expressed in terms of plasma frequency units (top scale) in order to compare with the O-mode ionogram traces which are based on the bottom scale. In order to keep the topside and ground-based sounding traces from overlapping, they are plotted using a scale (right) compressed by 1/2 of the altitude scale (left). The data correspond to 1651 UT, 10 June 1968. Adapted from Jackson et al. [1980].

trace labeled "Topside Sounding Trace". It is instructive to compare the ionogram traces (solid lines) with the corresponding portions of the vertical f_N profile (dashed line). (Note: in the ionosphere the wave energy travels with a speed less than c, thus the apparent range on the right scale is greater than the true range, converted to altitude, on the left scale; the right and left vertical scales have been adjusted for optimum comparison of the ionogram traces with the f_N profile.) The smooth topside (above 300 km) f_N profile produces a smooth ionogram trace with steep gradients near the wave cutoff (between 1 and 2 MHz) at the satellite altitude (1,000 km) and near the f_N peak (between 7 and 8 MHz). The structured E and F regions (dashed line below 300 km), however, produce major signatures on the corresponding (ground-based) ionogram trace. The local minimum at the E layer (called the E valley) produces a clear break in the ionogram trace. The minor inflection at the F_1 layer, produces a dramatic cusp in the ionogram trace. These signatures have become easy to recognize by ionospheric scientists and they provide instant insight of the reflecting medium. A similar situation is expected in the case of magnetospheric radio sounding using RPI on IMAGE.

3. Brief Review of Magnetospheric Remote Sensing Radio Techniques

Ground-based magnetospheric radio experiments date back to the work of *Storey* [1953] on highly dispersed very low frequency signals called whistlers that originate in lightning flashes. Whistlers observed at ground stations have been found to propagate along discrete geomagnetic field-aligned paths. These paths, or ducts, are formed by N_e irregularities in the direction perpendicular to **B** that are maintained all along the magnetic-field line from one hemisphere to the other. The frequency versus time, or dispersion, properties of a whistler can be used to determine both the ducting magnetic field line as well as N_e in the region of the path most distant from the Earth. Energy from a single lightning flash is regularly observed to travel along multiple paths, allowing the simultaneous probing of field lines corresponding to different latitudes. Much of the methodology for such passive magnetospheric probing with whistlers was developed during the IGY (the 18-month International Geophysical Year extending from June, 1957 through 1958) and immediately thereafter in the early 1960's. A variety of satellite techniques for interpreting dynamic whistler-mode spectra received in space were developed in the mid-to-late 1960's. From these and later studies, valuable information has been obtained in many areas including equatorial N_e profiles, global structure of the plasmasphere, ionosphere - magnetosphere plasma interchange, large scale plasma motions, whistler-mode propagation within ducts, and propagation in the nonducted mode and in the presence of multiple ion species. The investigations clearly revealed the important role whistlers play in wave-particle interactions - including the scattering of energetic electrons into the atmospheric loss cone.

In addition, there were many passive experiments involving ground- and satellite-based reception of magnetospheric VLF emissions due to hot plasma effects originating either spontaneously or by triggering. Others provided the first observations of resonant interactions between whistler-mode signals from Navy transmitters and energetic magnetospheric electrons.

References to this early magnetospheric radio research may be found in the classic book by *Helliwell* [1965] and in many review articles including those by *Smith and Brice* [1964], *Kimura* [1967] and *Carpenter* [1968]. Present day perspectives on various aspects of this research and on its later diagnostic applications may be found in *Sazhin et al*. [1992], *Sonwalkar* [1995], *Hayakawa* [1995], and *Lemaire and Gringauz* [1997].

One of the most favorable locations on Earth for passive whistler observations has been found to be near the 75^o west meridian in Antarctica. This location was also found to be favored for the injection of controlled VLF waves into the magnetosphere. Active experiments, conducted from Siple Station over a period of 15 years, provided a wealth of information on the problem of wave-particle energy and momentum exchange in the magnetosphere, including a threshold for exponential growth of coherent waves, saturation, and triggering of new frequencies (see, e.g., *Helliwell* [1988]). Information on the group delay and Doppler shift of signals from powerful VLF communication and navigation transmitters has been used to investigate several topics, including whistler-mode duct structure, plasma bulk motions, and temporal density variations of the

magnetospheric thermal plasma (see, e.g., *Thomson* [1981] and *Clilverd et al*. [1992]).

Exploratory magnetospheric sounding of plasma wave structures using high-power radar facilities has also been performed. *Gurevich et al*. [1992] reported receiving echoes from an altitude of about 4,000 km in the polar magnetosphere using the Sura HF heating facility operating at a frequency of 9.31 MHz with an effective radiating power of about 30 MW. They attributed the echoes to backscatter from ion acoustic turbulence in the field-aligned current region in this altitude region. Related experiments were performed earlier using ionospheric incoherent scatter facilities [*Foster et al.*, 1988; *Rietveld et al.*, 1991]. At times, these experiments recorded enhancements of the incoherent scatter spectrum so intense that they were attributed to contamination from hard targets such as satellites. Convincing arguments were made that the signal enhancements could be explained by the presence of ion acoustic waves. While these techniques do not promise to yield magnetospheric N_e values, they could yield valuable information on magnetospheric dynamics and plasma instability processes.

There have been a number of *in situ* active and passive magnetospheric radio experiments that have been used to obtain N_e. These have included a bistatic propagation experiment that measured the integrated N_e between the ISEE 1 and 2 satellites [*Harvey et al.*, 1979], a series of relaxation sounders, that measured the ambient N_e from the frequencies of plasma resonances and wave cutoffs (see eqs. 1-4) of sounder-stimulated emissions on ISEE 1, GEOS 1 and 2, and EXOS B and D [*Etcheto et al.*, 1983; *Oya and Ono*, 1987; *Oya et al.*, 1990], plasma wave receivers on Hawkeye, DE 1, and GEOTAIL that have been used to deduce ambient magnetospheric N_e values from naturally-produced emissions [*Calvert*, 1981a; *Persoon*, 1988] and map magnetospheric boundaries [*Matsumoto*, 1995], and thermal noise measurements to measure N_e and the electron temperature T_e [*Meyer-Vernet and Perche*, 1989]. The thermal noise technique is well adapted to measurements of N_e and T_e in the outer plasmasphere, the plasmapause and the cusp.

A radio sounder that will be capable of measuring both the ambient and remote N_e throughout the magnetosphere is now being prepared for flight. The next two sections describe the mission, the measurement capabilities of the sounder, and the feasibility of magnetospheric sounding.

4. The IMAGE Mission

IMAGE (Imager for Magnetopause-to-Aurora Global Exploration) has been selected to be NASA's first Medium-class-Explorer (MIDEX) mission. It has the scientific objective of providing an understanding of the global dynamics of the terrestrial magnetosphere in response to changing solar wind conditions. The mission was designed to answer the following questions: (1) What are the dominant mechanisms for injecting plasma into the magnetosphere on substorm and magnetic-storm time scales? (2) What is the directly driven response of the magnetosphere to solar wind changes? and (3) How and where are magnetospheric plasmas energized, transported, and subsequently lost during storms and substorms? Many of the processes related to these questions have time scales of the order of minutes to hours yet our present understanding of the magnetosphere is based on accumulated measurements taken over time scales of months to decades. The IMAGE instruments are designed to provide global images, on the time scale of minutes, of plasma processes at work throughout the magnetosphere from the plasmapause (the outer boundary of the high-density inner magnetosphere called the plasmasphere) to the magnetopause (the outer magnetospheric boundary). In high-latitude regions the images will include the polar cusp (the dayside region where solar-wind plasma readily enters and ionospheric plasma exits) and will extend down to the altitudes of brilliant auroral displays ($\approx$ 100 km). While the radio sounder on IMAGE will not provide global images in the same sense as the other imagers on the satellite, it will for the first time provide dynamic information (time scale of minutes) on the locations and shapes of important boundaries such as the magnetopause and plasmapause during the same time interval that global images are being collected by the other instruments. This capability, combined with the accumulated knowledge gained from magnetospheric modeling based on many decades of observations, promises to provide unprecedented insight into the plasma processes involved in the three questions listed above. For example, by measuring N_e profiles in

the polar cusp on one-minute time scales, it will be possible to determine whether solar-wind plasma entry is a steady-state or an impulsive process. Also, the effects of substorms on the loss of plasmaspheric ionization can be determined by monitoring the plasmapause N_e gradient.

IMAGE is scheduled to be launched into a highly elliptical polar orbit with an apogee geocentric distance of 8 R_E (the mean Earth radius, R_E, is 6,371 km) on January 1, 2000. IMAGE will make use of four imaging techniques: neutral atom imaging (NAI), extreme ultraviolet imaging (EUV), far ultraviolet imaging (FUV), and radio plasma imaging (RPI) during a two year mission. A brief description of the IMAGE mission can be found in *Green et al.* [1996] and the IMAGE Home Page at http://image.gsfc.nasa.gov.

Neutral atom imaging relies on the detection of neutral particles from the Earth's auroral zones, polar cusp and ring current. The neutral atoms are formed by charge exchange between magnetospheric ions and low-energy neutrals in these regions. The neutrals travel in straight lines from their place of origin to the point of their detection. They will be detected by a complement of three NAI instruments on the IMAGE satellite, producing images of the charge-exchange regions on a time scale of the order of minutes. This complement is composed of low energy (10 - 300 eV), medium energy (1 - 30 keV), and high energy (10 - 500 keV) neutral atom imagers (LENA, MENA and HENA, respectively).

The EUV (30.4 nm) imager will obtain images of the entire plasmaspheric distribution of He^+ in single exposures with angular resolutions of 0.6° and temporal resolutions of ten minutes and greater. The FUV imager will consist of three different detectors: (1) a set of three geocorona photometers (FUV/GEO), to determine the distribution of hydrogen atoms in the Earth's extended neutral atmosphere (the geocorona) by observing Lyman-alpha emissions (121.6 nm), (2) a spectrographic imager (FUV/SI) for separately measuring Doppler-shifted Lyman-alpha emissions (121.8 nm) (resulting from aurora emitted by charge-exchanged precipitating protons) and auroral-oxygen emissions at 135.6 nm, and (3) a wideband imaging camera (FUV/WIC) to image the aurora over the broad (140 - 190 nm) Lyman-Birge-Hopfield bands of N_2 for maximum day and night spatial resolution.

The RPI will consist of a swept-frequency digital radio sounder covering the frequency range from 3 kHz to 3 MHz (100 km to 100 m free-space wave length range) in order to measure the magnetospheric N_e from 0.1 to 10^5 cm^{-3}. The lowest frequencies will be used mainly for local soundings and thermal-noise measurements to determine ambient N_e values. Long-distance sounding to the magnetopause will generally involve $f \geq$ about 30 kHz, i.e., to targets with $N_e \geq$ about 10 cm^{-3}. It is called an imager rather than a sounder because in addition to measuring echo signal strength and delay time as a function of sounding frequency, as in traditional ionospheric topside sounders (but with greater sensitivity than these earlier sounders), it will be capable of measuring the echo direction-of-arrival and Doppler spectrum. Thus the RPI will be able to produce maps of the echoing structures. Most of the RPI soundings will be taken near the 8 R_E apogee radial distance between 45 and 90° north geographic latitude. In this region, the spacecraft will be immersed in a magnetospheric N_e cavity extending from the plasmapause to the magnetopause as illustrated in Figure 2. Ionospheric sounding of the ionospheric N_e peak shown in the bottom of the figure was briefly discussed in Section 1. It was discussed from the point-of-view of ground-based sounding (to investigate the region below the peak N_e in Figure 1), and topside sounding from satellites (to investigate the region from the peak N_e up to the satellite altitude of 1,000 km in Figure 1 which is well below the plasmapause in Figure 2). Because of the unique location of IMAGE in the magnetospheric N_e cavity, it will simultaneously perform magnetospheric sounding upward to the magnetopause and downward to the plasmapause. This type of sounding has been discussed in a number of publications [*Reiff et al.*, 1994a; *Reiff et al.*, 1994b; *Calvert et al.*, 1995; *Fung and Green*, 1996; *Green et al.*, 1996; *Reiff et al.*, 1996; *Green et al.*, 1998] and will be described in more detail in the next section.

5. Magnetospheric Radio Sounding from IMAGE

The RPI on IMAGE will have capabilities similar to modern state-of-the-art ground-based digital ionospheric sounders[*Reinisch*, 1996]. It will be capable of measuring the following information associated with the received echo resulting from a transmitted pulse:

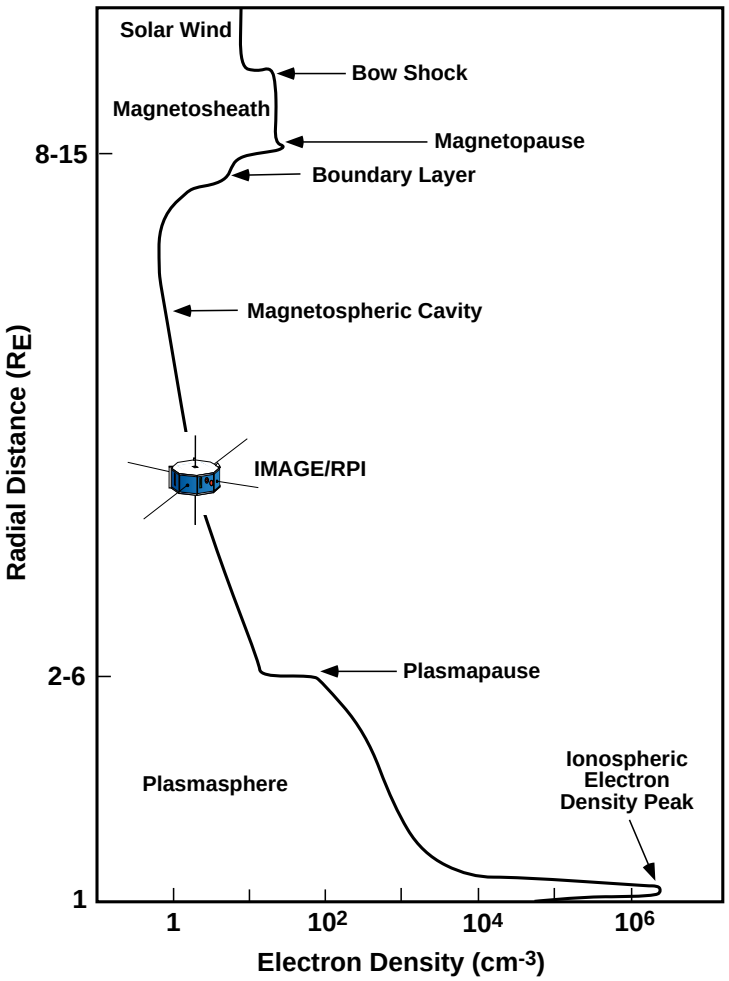

Figure 2. Schematic illustration of the IMAGE spacecraft in the magnetospheric N_e cavity extending from the plasmapause to the magnetopause. The RPI on IMAGE will be able to simultaneously perform radio sounding upward toward the magnetopause and downward toward the plasmapause.

frequency, time delay, amplitude, phase, Doppler spectrum, polarization and direction-of-arrival. (Only the first three were measured by the Alouette and ISIS analog topside sounders.) RPI will use two mutually orthogonal 500-m tip-to-tip dipoles in the IMAGE spin plane for transmission. These antennas will also be used for reception as will a third 20 m tip-to-tip length dipole along the spin axis. The IMAGE spacecraft will rotate in the cartwheel mode, i.e., with its spin axis normal to the orbit plane, with a spin rate of 0.5 rpm. This spin rate will be achieved with full deployment of the thin (0.4 mm) BeCu 28 gauge 7-strand non-insulated wire spin-plane antennas in a time period on the order of one month after launch by alternately deploying the antenna wires and spinning up the spacecraft using magnetic torquing near perigee (1,000 km altitude). It will be possible to transmit all the energy either in the R-X or L-O polarization relative to the satellite spin vector in order to reduce the antenna-pattern nulls in the spin plane. On-board digital signal-processing techniques (coherent pulse compression and Doppler integration) will be used to increase the signal-to-noise ratio. The RPI sounder data will be used to produce N_e profiles and echo maps of N_e structures. Such techniques are currently in use by a global network of ground-based digital ionospheric sounders [*Reinisch et al.*, 1995; *Scali et al.*, 1995]. The ionospheric sky maps are produced by these ground-based sounders by first separating the echoes from various moving N_e irregularities by their different Doppler shifts and then using an array of spaced antennas to determine directions of arrival. The concept used by RPI on IMAGE will be similar but the Doppler shifts will be due to the relative velocity between the moving plasma reflecting surface and the moving spacecraft, and the directions of arrival will be determined from the amplitude and phase measurements of the signals received on the three orthogonal antennas.

The RPI will be able to determine the distances to the magnetopause, plasmapause and other magnetospheric N_e structures, such as the polar cusp. It will also determine the corresponding N_e values at these boundaries. In addition, it will be able to simultaneously determine the N_e profiles leading up to some of them. Since N_e increases inward from the plasmapause, echoes at higher frequencies will arrive from deep within the plasmasphere. These echoes will enable N_e profiles to be deduced on time scales of minutes, much shorter than the typical time scales involved in magnetospheric dynamics. They will be obtained in the directions of increasing N_e gradients and, at times, it will be possible to simultaneously deduce N_e profiles in different directions.

Simulated magnetospheric echoes received by RPI are presented in Figure 3 as solid lines. The simulation assumes that IMAGE is located at a radial distance of 6 R_E along a radial line from the center of the Earth at 25° magnetic latitude. It is based on a three-dimensional magnetospheric N_e model. The dashed line shows the variation of f_N along a radius that passes through the IMAGE satellite. This figure is analogous to Figure 1 for the ionospheric case. As in Figure 1, the

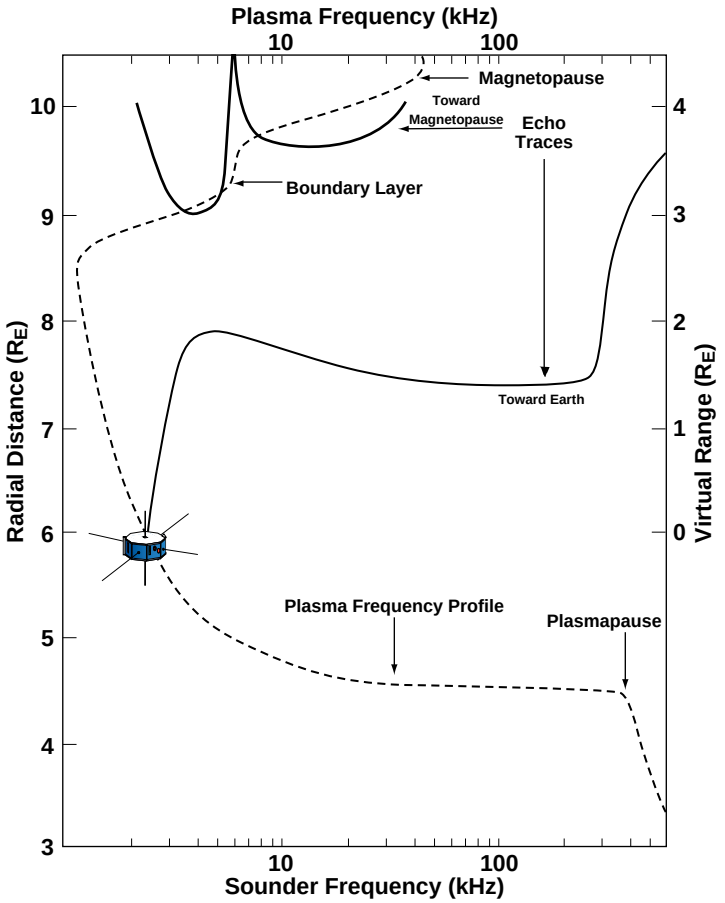

Figure 3. Similar to Figure 1, except in this magnetospheric case, the O-mode echo traces are simulated using ray tracing, including refraction effects, based on a sounder located at a radial distance of 6 R_E at 25° magnetic latitude in a 3-D N_e model.

N_e profile is expressed in terms of f_N (top scale) so as to directly compare with the echo traces. There are three important differences, however, between these figures. First, in the ionospheric case of Figure 1 the profile was derived from existing ionospheric data, whereas in the magnetospheric situation of Figure 3 the comparable data do not exist and the RPI radio-reflection traces were simulated based on 3-D ray-tracing.

The second difference between Figures 1 and 3 is that the observed reflection traces for the ionosphere in Figure 1 correspond to two different sounders whereas the simulated magnetospheric reflection traces in Figure 3 correspond to a single sounder. In the ionospheric case in Figure 1 an N_e peak is under investigation and two sounders are required, one above and one below the N_e peak altitude. In the magnetospheric case in Figure 3 an N_e valley is under investigation and only one sounder (in the valley) is required. The magnetospheric reflection trace in Figure 3 from the direction of the plasmapause (labeled "Toward Earth") is analogous to the ionospheric topside trace in Figure 1. The traces are inverted relative to one another because the virtual range increases downward in the case of the topside-sounder presentation of Figure 1 and upward in the case of the "Toward Earth" simulated RPI echo trace in Figure 3. They both extend from the wave cutoff condition at the satellite (zero virtual range) to the frequency corresponding to the maximum f_N. The simulated RPI magnetospheric trace in Figure 3 from the direction toward the magnetopause is analogous to the ionospheric ground-based sounding F region trace in Figure 1. The magnetospheric trace in this case starts at a large apparent range (rather than zero) because the transmitted wave going toward the magnetopause initially propagates into a region of decreasing N_e. It has to travel some distance before it encounters an N_e value capable of causing total reflection. The delay time then decreases with increasing frequency for a short frequency interval (even though the wave is penetrating deeper into the medium) because the wave propagation speed increases as the frequency increases.

The third difference between these figures becomes apparent when comparing the virtual range scales on the right side with the distance scales on the left side in each case. Aside from the change in direction on the right-hand side (as described above), there is a major difference in the magnitude of the scales. In the ionospheric situation of Figure 1, the virtual range (right) and true distance (left) scales differ by a factor of two and the virtual distance to a particular feature on the reflection trace is usually considerably greater than the true distance to the corresponding feature on the ionospheric f_N profile. In the magnetospheric situation of Figure 3, these scales are the same and the virtual distance to a particular feature on the reflection trace is often comparable to the true distance to the corresponding feature on the magnetospheric f_N profile. These differences are attributed to the differences in the relative geometry between the directions of the profile and the echoes in each case. In the ionospheric situation (Figure 1), where the ionosphere is assumed to be horizontally stratified, the echoes are vertical and are aligned along the vertical f_N profile. In the magnetospheric situation (Figure 3), the radial direction of the f_N pro-

file (which crosses the IMAGE satellite position) does not generally coincide with the normals to the f_N contours. Thus the directions of the echoes, which coincide with these normals at the reflecting location, will be different than the direction corresponding to the f_N profile in Figure 3. In addition, the long distances with conditions of low N_e in the magnetospheric case (where the operating frequency will often be much greater than f_N) decrease the difference between virtual and true range.

In Figure 3 the sounder reflection traces were simulated using the ray-tracing modeling code of Green [1988], which includes refraction effects, based on a 3-D N_e model. When RPI flies on IMAGE, N_e profiles will be deduced from the reflection traces using inversion techniques [*Jackson*, 1969; *Huang and Reinisch*, 1982] as was done in the case of the ionospheric soundings of Figure 1. As IMAGE travels along its orbit it will be possible to construct N_e contours in the orbital plane as was done in the topside ionosphere using the Alouette and ISIS satellites [*Warren*, 1969] even during intense auroral kilometric radiation [*Benson and Akasofu*, 1984]. RPI will also provide information on distortions of the geomagnetic field from the reception of ducted echoes propagating along magnetic field-aligned paths of N_e irregularities [*Calvert*, 1981b]. In addition to these remote measurements, the RPI on IMAGE will provide accurate *in situ* N_e measurements, down to the instrumental lower frequency limit of 3 kHz (corresponding to N_e of 0.1 cm^{-3}), from sounder-stimulated plasma resonances [*Benson*, 1977] and thermal noise measurements [*Meyer-Vernet and Perche*, 1989]. The latter technique also provides the electron temperature.

One of the greatest contributions of RPI to the IMAGE mission will be the capability to produce echo maps of N_e structures in the vicinity of important boundaries such as the magnetopause, polar cusp and plasmapause on time scales of minutes. As pointed out earlier, similar maps are routinely produced by modern ground-based sounders. A sequence of N_e echo maps will be produced over intervals on the order of hours, in the apogee portion of the IMAGE orbit (period about 13 h). They will provide unprecedented information on magnetopause dynamics while other IMAGE instruments obtain global images of the inner magnetosphere. In addition, the plasmaspheric N_e profiles obtained from the RPI during these long time intervals will provide a degree of "ground truth" information for these global images. These profiles will be used to follow the dynamic erosion and later filling of magnetic flux tubes. Plasmaspheric erosion is believed to be driven by the penetration of a strengthened convection electric field and interaction with newly injected ring current populations following substorm onset. Flux tube filling involves a complex interplay between ionospheric outflow and heating at high altitudes. The RPI real-time monitoring of the absolute electron densities in the outer plasmasphere, together with the EUV and ENA images, will provide a global insight into the nature of these processes for the first time.

Calvert et al. [1995] considered the feasibility of performing such measurements with a radio sounder in the magnetosphere. This study included the effects of curved targets as seen by a sounder located between the plasmapause and the magnetopause. In this situation there is a decreased echo power return from the convex plasmapause (defocusing) and an increased echo power return from the concave magnetopause (focusing). The decreased power return at the plasmapause due to defocusing is not much of a problem for RPI on IMAGE because the plasmapause marks a region of increasing N_e with increasing distance from the spacecraft and thus frequencies where the RPI antennas operate at their greatest efficiency will be used.

The magnetopause is a challenging radio sounding target because the low electron density there (see Figure 1) requires sounding frequencies which will be well below 100 kHz most of the time. In this frequency range the transmitted power is proportional to f^4 and even the long 500-m dipoles are very inefficient radiators at such low frequencies (they become shorter than 1/2 the vacuum wavelength at frequencies below 300 kHz). The RPI radiated power at 30 kHz will be about 50 mW (corresponding to a rms voltage at the root of the antennas of 3 kV from the 10 W transmitter). As a point of comparison, the highly successful ISIS 1 and 2 ionospheric topside-sounders would radiate 50 mW at about 280 kHz (based on Equation (20) of *Calvert et al*. [1995] using 1 kV (from a 400 W transmitter) and a 73.2 m tip-to-tip, 13 mm diameter, stem dipole). (Note: the ISIS satellites each used two antenna lengths to cover the frequency range from 100 kHz to 20 MHz.) Of course the ISIS ionospheric sounding distances were

considerably less than the magnetospheric sounding distances to be overcome by the RPI and the ISIS long-distance sounding was mainly performed at higher frequencies corresponding to greater antenna efficiency.

Nevertheless, there are several additional factors (in addition to the above-mentioned longer antennas and higher antenna voltage) that greatly enhance the capability of RPI (for long-distance sounding to the magnetopause) relative to ISIS (for ionospheric sounding). Namely, RPI will benefit from (1) several dB of echo signal gain from magnetopause focusing, (2) a 22 dB gain from a smaller receiver bandwidth (300 Hz compared with 50 kHz on ISIS) so the received echo power competes with less noise power, (3) a 3 dB gain from using two transmitters that drive the two spin-plane dipoles $\pm 90°$ out of phase in order to transmit waves with R-X or L-O polarization (ISIS used one transmitter, and one receiver, into one of two dipoles depending on the transmission frequency); on reception, the simultaneous use of orthogonal antennas will eliminate polarization fading of the received signals and will enable wave polarization discrimination of these signals in order to aid in the interpretation of the echoes, (4) a set of three mutually orthogonal antennas for direction finding (ISIS did not have a spin-axis antenna), (5) double tuning at the receiver inputs to reduce the risk of saturation by out-of-band signals, and transmit antenna tuning to aid in obtaining the 3 kV antenna voltage (ISIS did not use antenna tuning), (6) coherent pulse compression and (7) Doppler integration. The gain from the last two depend on the wave form being used, it was 21 dB in the example discussed by *Calvert et al.*[1995]. They are well-proven digital signal processing techniques used by a large number of ground-based ionospheric sounders. They could not be employed by the ISIS topside sounders because the detected receiver video output signal was used rather than the entire waveform. Coherent pulse compression, which correlates the transmitted and received pulses, allows long low-power pulses to be transmitted without sacrificing echo-range resolution. Doppler integration is based on transmitting M pulses (e.g., M = 8 or 16) at the same frequency and calculating separate Fourier transforms from the sequence of M time samples taken at the same echo delay after each pulse (and repeating the process for each echo-delay increment). It is routinely used to map the motions of ionospheric N_e irregularities in the dynamic high-latitude regions even in the presence of severe spread F (a condition where N_e irregularities distributed throughout the ionospheric F region produce many echoes that result in the spreading of the F-layer reflection trace over a broad area on the ionogram trace) [*Reinisch et al.*, 1995]. It is expected that the magnetosphere will also contain large-scale regions of N_e irregularities that will be detected in a similar way by the RPI.

Calvert et al. [1995] concluded that a sounder of the type planned for RPI on IMAGE could make N_e measurements of magnetospheric structures with 10% accuracy, a range resolution of 500 km and an angular resolution of 4° at magnetopause target distances of 4 R_E on a time scale of about three minutes. This claim has generated some debate in the scientific community [*Greenwald*, 1997a; *Calvert et al.*, 1997; *Greenwald*, 1997b]. It is worthwhile to note when considering such discussions, that *Calvert et al.* [1995] considered a model magnetopause centered at a radial distance of 10 R_E with a sounder at a radial distance of 6 R_E, whereas the apogee of the IMAGE orbit will be at 8 R_E. Thus, the sounding distance to a 10 R_E magnetopause for RPI will be 1/2 the magnetopause/sounder distance used in the feasibility study of *Calvert et al.* [1995] corresponding to a four-fold increase in echo power (6 dB) over what was considered in that study. In addition, *Calvert et al.* [1995] discussed only one specific waveform as an example to illustrate how pulse compression and spectral integration enhance magnetospheric radio imaging. The RPI instrument to fly on IMAGE will use different transmission waveforms that will be selectively used to satisfy different measurement objectives.

Since these waveforms are considerably different from those that have been previously used in topside ionospheric sounding, e.g., in the Alouette/ISIS program, a brief description of them will be given here. The RPI will predominantly use three different waveforms: (1) complementary phase coded pulse sequences, (2) staggered pulse sequences and (3) frequency-modulated (or "chirp") pulses. Each of these transmission waveforms has advantages and disadvantages. Under certain circumstances two or even all three waveforms will be used to observe and resolve details of the structure and dynamics of the reflecting plasma.

The first waveform will be used with pulse repetition rates PRR between 0.5 to 4.0 pulses per second. The former rate corresponds to an inter-pulse period of

2 s and, assuming pulses of length 16 x 3.2 = 51.2 ms (where 3.2 ms is the "chip" length of the phase code), will allow virtual ranges (ct/2) to be measured from distances ranging from slightly more than 1 R_E to almost 46 R_E (a maximum delay time of 2 - 15 x 0.0032 s is used since the last 15 phase-code samples before the next sounder pulse do not contain the complete pulse phase code). The maximum range in the case of the 4 pps rate is reduced to slightly less than 5 R_E. In either case, the target range resolution is defined by the compressed pulse width of 3.2 ms corresponding to 480 km or less than 0.1 R_E. While the latter case with the higher PRR is limited to shorter ranges, it is capable of measuring larger Doppler frequencies f_D and hence higher radial velocities v_r given by

$$v_r = \lambda f_D/2 \qquad (5)$$

where λ is the free-space wavelength [*Flock*, 1979]. The maximum unambiguous f_D is limited by the Nyquist sampling criterion to one half the data sampling rate DSR, i.e., f_D < DSR/2. When using complementary phase coded pulse sequences, the data sampling rate becomes DSR = PRR/2 because the pulse-compressed data from two transmitted pulses are summed (in order to reduce signal leakage into other range bins). Thus, the maximum unambiguous f_D becomes f_D = PRR/4 and the maximum v_r that can be measured is λPRR/8. For an operating frequency of 30 kHz, expected to be used for magnetopause sounding, the maximum radial velocities are 0.3 and 5 km/s for PRR = 0.5 and 4.0 pps, respectively. Since quadrature samples (sometimes called sine and cosine samples) of the intermediate frequency are made, the sign of the Doppler shift (and hence of v_r) will also be determined. Thus the first waveform will be limited to probing plasma structures moving relative to the satellite with speeds of less than 5 km/s when sounding at 30 kHz. During sections of the orbit where the spacecraft moves essentially parallel to the magnetopause N_e contours, good results will be obtained if the boundaries are not moving too quickly toward or away from the satellite. These boundary relative-motion constraints become even more severe (by an order-of-magnitude) near the plasmapause where the higher N_e values will require sounding frequencies around 300 kHz.

These limitations in the Doppler measurements will be overcome by using the second waveform. The staggered pulse sequence used in this case consists of unevenly spaced 3.2 ms pulses. The transmission-pulse time slots are m x 3.2 ms with m values varying from 1 to 768. In order to leave sufficient space for the reception of echoes, not all m values are used. On each sounding frequency a total of about 300 pulses will be transmitted and special correlation techniques will be used to determine the spectra at each of up to 128 ranges. The staggered-pulse-sequence waveform is designed to provide a maximum unambiguous f_D = 150 Hz (corresponding to the maximum data sampling rate of 1/0.0032). From equation (5), it is seen that this capability leads to the detection of a maximum relative v_r of 750 km/s at 30 kHz. Such capabilities should allow radio imaging of the magnetopause even during the presence of wave-like magnetopause structures with amplitudes of thousands of kilometers and radial motions as large as 150 km/sec as reported by *Safrankova et al.* [1997] based on data from the Russian satellite - Czech subsatellite pair INTERBALL 1/ MAGION 4. In the case of plasmapause sounding at 300 kHz, radial motions up to about 75 km/s could be detected which is far in excess of anything likely to be sustained for more than a few minutes at most.

Although waveform (2) has great capabilities in highly dynamic conditions, it also has some limitations. Some of the received echoes may be lost because they arrive during the transmission of one of the later pulses. This situation leads to range and Doppler leakage that cannot be totally resolved by the software. Such problems, occurring during conditions of high Doppler shift, will be resolved by employing the third waveform based on chirp pulses. These pulses will have a linear frequency modulation and the target range is obtained from the beat frequency of the received and transmitted signals. In the case of the RPI, the range accuracy will be 300 km for the chirp waveform. The ability to detect an echo from a transmitted chirp signal is not affected by high Doppler shifts. Such shifts, however, introduce target range errors since the Doppler shift will be added to the beat frequency. For the RPI chirp waveform, a Doppler shift of 5 Hz will result in a range error of 300 km. Range and Doppler ambiguity can be resolved when RPI successively transmits two or three of the available waveforms at each frequency.

It must be kept in mind that the first waveform is

not restricted to pulse lengths of 16 x 3.2 = 51.2 ms, and that pulses with 1 x, 2 x, 4 x and 8 x 3.2 ms may be used under highly dynamic condition, i.e., when the conditions of the reflecting medium are changing on a time scale shorter than the probing pulse time duration.

Eliminating range and Doppler ambiguities by using the above procedures will be at the cost of temporal and/or spatial resolution. Thus it is planned that such muti-mode operations will be periodically scheduled among normal single-mode operations in a manner so as to maximize resolution while minimizing ambiguity. These capabilities will make the RPI to fly on IMAGE even more capable than the magnetospheric sounder discussed by *Calvert et al*. [1995].

6. Summary

A wealth of magnetospheric N_e information (as well as information on magnetospheric wave-particle energy and momentum exchange) has been obtained from more than four decades of ground-based experiments involving whistler-mode waves. These remote radio observations have been complemented by *in situ* measurements involving numerous satellites. Though the resulting accumulated knowledge is substantial, and has provided an important base for understanding the general problem of the interaction of planetary magnetospheres with a stellar wind, many major questions remain concerning the complex physics of the global response of the terrestrial magnetosphere to the dynamic nature of the solar wind.

Radio plasma Imaging with RPI during the IMAGE mission will apply state-of-the-art digital sounding techniques, in routine use in ground-based ionospheric sounding, to the investigation of the magnetosphere. The resulting high time-resolution measurements of distant N_e structures will provide critical information needed to resolve fundamental magnetospheric problems. Combining the RPI boundary locations, N_e profiles and echo maps of N_e structures with images from the other IMAGE remote sensing instruments will produce dynamic global descriptions of fundamental magnetospheric processes.

References

Appleton, E. V. and M. A. F. Barnett, On some direct evidence for downward atmospheric reflection of electric rays, *Proc. R. Soc. Lond., 109A*, 621-641, 1925.

Benson, R. F., Stimulated plasma waves in the ionosphere, *Radio Sci., 12*, 861-878, 1977.

Benson, R. F., Ionospheric investigations using digital Alouette/ISIS topside ionograms, in *1996 Ionospheric Effects Symposium*, edited by J. M. Goodman, pp. 202-209, Alexandria, Virginia, 1996.

Benson, R. F. and S.-I. Akasofu, Auroral kilometric radiation/aurora correlation, *Radio Sci., 19*, 527-541, 1984.

Breit, G. and M. A. Tuve, A test for the existence of the conducting layer, *Phys. Rev., 28*, 554-575, 1926.

Budden, K. G., *The propagation of radio waves, the theory of radio waves of low power in the ionosphere and magnetosphere*, 669 pp., Cambridge University Press, New York, 1985.

Calvert, W., The auroral plasma cavity, *Geophys. Res. Lett., 8*, 919-921, 1981a.

Calvert, W., The detectability of ducted echoes in the magnetosphere, *J. Geophys. Res., 86*, 1609-1612, 1981b.

Calvert, W., R. F. Benson, D. L. Carpenter, S. F. Fung, D. L. Gallagher, J. L. Green, D. M. Haines, P. H. Reiff, B. W. Reinisch, M. F. Smith and W. W. L. Taylor, The feasibility of radio sounding in the magnetosphere, *Radio Sci., 30*, 1577-1595, 1995.

Calvert, W., R. F. Benson, D. L. Carpenter, S. F. Fung, D. L. Gallagher, J. L. Green, D. M. Haines, P. H. Reiff, B. W. Reinisch, M. F. Smith and W. W. L. Taylor, Reply, *Radio Sci., 32*, 281-284, 1997.

Carpenter, D. L., Recent research on the magnetospheric plasmapause, *Radio Sci., 3*, 719, 1968.

Clilverd, M. A., A. J. Smith and N. R. Thomson, The

effects of ionospheric horizontal electron density gradients on whistler mode signals, *J. Atm. and Terr. Phys.*, *54*, 1061-1074, 1992.

Etcheto, J., G. Belmont, P. Canu and J. G. Trotignon, Active sounder experiments on GEOS and ISEE, in *Active Experiments in Space, Proceedings of an International Symposium held at Alpbach, Austria 24-28 May 1983, ESA SP-195*, pp. 39-46, European Space Agency, Noordwijk, Netherlands, 1983.

Flock, W. L., *Electromagnetics and the Environment: Remote Sensing and Telecommunications*, 325 pp., Prentice-Hall, Inc., Englewood Cliffs, New Jersey, 1979.

Foster, J. C., C. d. Pozo, K. Groves and J.-P. S. Maurice, Radar observations of the onset of current driven instabilities in the topside ionosphere, *Geophys. Res. Lett*, *15*, 160-163, 1988.

Franklin, C. A. and M. A. Maclean, The design of swept-frequency topside sounders, *Proc. IEEE, 57*, 897-929, 1969.

Fung, S. F. and J. L. Green, Global imaging and remote sensing of the magnetosphere, in *Radiation Belts: Models and Standards*, Geophysical Monograph 97, pp. 285-290, American Geophysical Union, Washington, D.C., 1996.

Goertz, C. K. and R. J. Strangeway, Plasma waves, in *Introduction to Space Physics*, edited by M. G. Kivelson and C. T. Russell, pp. 356-399, Cambridge University Press, New York, 1995.

Green, J. L., Ray tracing of planetary radio emissions, in *Planetary Radio Emissions II, Proceedings of the 2nd international workshop*, pp. 355-379, Graz, Austria, 1988.

Green, J. L., S. F. Fung and J. L. Burch, Application of magnetospheric imaging techniques to global substorm dynamics, in *Proc. Third International Conference on Substorms (ICS-3), ESA SP-389*, edited by E. J. Rolfe and B. Kaldeich, pp. 655-661, European Space Agency, Versailles, 1996.

Green, J. L., W. W. L. Taylor, S. F. Fung, R. F. Benson, W. Calvert, B. Reinisch, D. L. Gallagher and P. H. Reiff, Radio remote sensing of magnetospheric plasmas, Measurement Techniques for Space Plasmas: Fields, Geophysical Monograph 103, pp. 193-198, American Geophysical Union, Washington, D.C., 1998.

Greenwald, R. A., Comment on "The feasibility of radio sounding in the magnetosphere" by W. Calvert et al., *Radio Sci.*, *32*, 277-280, 1997a.

Greenwald, R. A., Rebuttal to reply by W. Calvert et al., *Radio Sci.*, *32*, 877-879, 1997b.

Gurevich, A. V., A. M. Babichenko, A. N. Karashtin and V. O. Rapoport, HF sounding of the auroral magnetosphere, *J. Geophys. Res.*, *97*, 8693-8696, 1992.

Harvey, C. C., J. Etcheto and A. Mangeney, Early results from the ISEE electron density experiment, *Space Sci. Rev.*, *23*, 39-58, 1979.

Hayakawa, M., Whistlers, in *Handbook of Atmospheric Electrodynamics*, *2*, edited by H. Volland, pp. 155-193, CRC Press, Boca Raton, Florida, 1995.

Helliwell, R. A., *Whistlers and Related Ionospheric Phenomena*, 349 pp., Stanford University Press, Stanford, California, 1965.

Helliwell, R. A., VLF wave stimulation experiments in the magnetosphere from Siple Station, Antarctica, *Rev. Geophys.*, *26*, 551-578, 1988.

Huang, X. and B. W. Reinisch, Automatic calculation of electron density profiles from digital ionograms 2. True height inversion of topside ionograms with the profile-fitting method, *Radio Sci.*, *17*, 837-844, 1982.

Hunsucker, R. D., *Radio techniques for probing the terrestrial ionosphere*, Phys. Chem. Space, Vol. 22, 293 pp., Springer, Berlin, 1991.

Jackson, J. E., The reduction of topside ionograms to electron-density profiles, *Proc. IEEE*, *57*, 960-976, 1969.

Jackson, J. E., *Alouette-ISIS Program Summary*, NSSDC Report 86-09, National Space Science Data Center, Greenbelt, Maryland, 1986.

Jackson, J. E., E. R. Schmerling and J. H. Whitteker, Mini-review on topside sounding, *IEEE Trans. Antennas Propagat., AP-28*, 284-288, 1980.

James, H. G., The OEDIPUS-C experiment and its results, *Eos Trans. AGU, 77*, April 23, 1996 Supplement, S200, 1996.

Kimura, I., On observations and theories of the VLF emissions, *Planet Space Sci., 15*, 1427-1462, 1967.

Lemaire, J. F. and K. I. Gringauz, *The Earth's Plasmasphere*, in press, Cambridge Press, 1997.

Matsumoto, H., Can we probe the magnetotail structure using plasma wave data? : GEOTAIL observations, Paper GAA22E presented at the XXI General Assembly of IUGG in Boulder Colorado, July 2-14, 1995.

Meyer-Vernet, N. and C. Perche, Tool kit for antennae and thermal noise near the plasma frequency, *J. Geophys. Res., 94*, 2405-2415, 1989.

Oya, H., A. Morioka, K. Kobayashi, M. Iizima, T. Ono, H. Miyaoka, T. Okada and T. Obara, Plasma wave observation and sounder experiments (PWS) using the Akebono (EXOS-D) satellite - Instrumentation and initial results including discovery of the high altitude equatorial plasma turbulence, *J. Geomagn. Geoelectr., 42*, 411-442, 1990.

Oya, H. and T. Ono, Stimulation of plasma waves in the magnetosphere using satellite JIKIKEN (EXOS-B). Part II: Plasma density across the plasmapause, *J. Geomagn. Geoelectr., 39*, 591-607, 1987.

Persoon, A. M., Electron density distributions in the high-latitude magnetosphere, *Adv. Space Res., 8*, 79-88, 1988.

Pulinets, S. A., Prospects of topside sounding, in *WITS handbook N2*, edited by C. H. Liu, pp. 99-127, SCOSTEP Publishing, Urbana, Illinois, 1989.

Reiff, P. H., J. L. Green, R. F. Benson, D. L. Carpenter, W. Calvert, S. F. Fung, D. L. Gallagher, B. W. Reinisch, M. F. Smith and W. W. L. Taylor, Radio imaging of the magnetosphere, *Eos Trans. AGU, 75*, 129-134, 1994a.

Reiff, P. H., J. L. Green, R. F. Benson, D. L. Carpenter, W. Calvert, S. F. Fung, D. Gallagher, Y. Omura, B. W. Reinisch, M. F. Smith and W. W. L. Taylor, Remote sensing of substorm dynamics via radio sounding, in *Substorms 2, Proceedings of the Second International Conference on Substorms*, edited by J. R. Kan, J. D. Craven and S.-I. Akasofu, pp. 281-287, University of Alaska Press, Fairbanks, 1994b.

Reiff, P. H., C. B. Boyle, J. L. Green, S. F. Fung, R. F. Benson, W. Calvert and W. W. L. Taylor, Radio Sounding of Multiscale Plasmas, in *Physics of Space Plasmas, 14*, edited by T. Chang and J. R. Jasperse, pp. 415-429, Cambridge, MA, 1996.

Reinisch, B. W., Modern Ionosondes, in *Modern Ionospheric Science*, edited by H. Kohl, R. Ruster and K. Schlegel, European Geophysical Society, pp. 440-458, Katlenburg-Lindau, Germany, 1996.

Reinisch, B. W., T. W. Bullett, J. L. Scali and D. M. Haines, High latitude digisonde measurements and their relevance to IRI, *Adv. Space Res., 16*, (1)17-(1)26, 1995.

Rietveld, M. T., P. N. Collis and J.-P. St.-Maurice, Naturally enhanced ion acoustic waves in the auroral ionosphere observed with the EISCAT 933-MHz radar, *J. Geophys. Res., 96*, 19,291-19,305, 1991.

Safrankova, J., Z. Nemecek, L. Prech, D. Sibeck, G. Zastenker, A. Skalsky and N. Rybeva, Magnetopause shape and motion under sudden changes of the solar wind parameters, *Eos Trans. AGU, 78*, April 29,1997 Supplement, S292, 1997.

Sazhin, S. S., M. Hayakawa and K. Bullough, Whistler diagnostics of magnetospheric parameters: a review, *Ann. Geophys., 10*, 293-308, 1992.

Scali, J. L., B. W. Reinisch, C. J. Heinselman and T. W. Bullett, Coordinated digisonde and incoherent scatter radar F region drift measurements at Sondre Stromfjord,

Radio Sci., *30*, 1481-1498, 1995.

Smith, R. L. and N. Brice, Propagation in multicomponent plasmas, *J. Geophys. Res.*, *69*, 5029-5040, 1964.

Sonwalkar, V. S., Magnetospheric LF-, VLF-, and ELF-waves, in *Handbook of Atmospheric Electrodynamics*, edited by H. Volland, pp. 407-462, CRC Press, Boca Raton, Florida, 1995.

Storey, L. R. O., An investigation of whistling atmospherics, *Phil. Trans. Roy. Soc.*, *246*, 113-141, 1953.

Thomson, N. R., Whistler mode signals: spectrographic group delays, *J. Geophys. Res.*, *86*, 4795-4802, 1981.

Warren, E. S., The topside ionosphere during geomagnetic storms, *Proc. IEEE*, *57*, 1029-1036, 1969.